Reduced Efficacy of the Plk1 Inhibitor BI 2536 on the Progression of Hepatocellular Carcinoma due to Low Intratumoral Drug Levels[1,2]

Jörg Haupenthal[*,3,4], Verena Bihrer[*,4], Huedayi Korkusuz[†], Otto Kollmar[‡], Christian Schmithals[*], Susanne Kriener[§], Knut Engels[§], Thomas Pleli[*], Alexander Benz[§], Marta Canamero[¶], Thomas Longerich[#], Bernd Kronenberger[*], Swantje Richter[**], Oliver Waidmann[*], Thomas J. Vogl[†], Stefan Zeuzem[*] and Albrecht Piiper[*]

*Department of Medicine I, Johann Wolfgang Goethe University, Frankfurt, Germany; †Department of Diagnostic and Interventional Radiology, Johann Wolfgang Goethe University, Frankfurt, Germany; ‡Department of General, Visceral, Vascular and Pediatric Surgery, University of Saarland, Homburg, Germany; §Department of Pathology, University of Frankfurt, Frankfurt, Germany; ¶Comparative Pathology Unit, Centro Nacional de Investigaciones Oncologicas, Madrid, Spain; #Institute of Pathology, University of Heidelberg, Heidelberg, Germany; **Institute of Biostatistics and Mathematical Modelling, University of Frankfurt/M, Frankfurt, Germany

Abstract

Highly promising preclinical data obtained in cultured cells and in nude mice bearing xenografts contrast with the rather modest clinical efficacy of Polo-like kinase 1 (Plk1) inhibitors. In the present study, we investigated if Plk1 might be a suitable target in hepatocellular carcinoma (HCC) and if a genetically engineered mouse tumor model that well reflects the tumor cell and micro-environmental features of naturally occurring cancers might be suitable to study anti-Plk1 therapy. Analysis of Plk1 expression in human HCC samples confirmed that HCC express much higher Plk1 levels than the adjacent normal liver tissue. Inhibition of Plk1 by an adenovirus encoding for a short hairpin RNA against Plk1 or by the small-molecule inhibitor BI 2536 reduced the viability of HCC cell lines and inhibited HCC xenograft progression in nude mice. Treatment of transforming growth factor (TGF) α/c-myc bitransgenic mice with BI 2536 during hepatocarcinogenesis reduced the number of dysplastic foci and of Ki-67–positive cells within the foci, indicating diminished tumorigenesis. In contrast, BI 2536 had no significant effect on HCC progression in the transgenic mouse HCC model as revealed by magnetic resonance imaging. Measurement of BI 2536 by mass spectrometry revealed considerably lower BI 2536 levels in HCC compared with the adjacent normal liver tissue. In conclusion, low intratumoral levels are a novel mechanism of resistance to the Plk1 inhibitor BI 2536. Plk1 inhibitors achieving sufficient intratumoral levels are highly promising in HCC treatment.

Neoplasia (2012) 14, 410–419

Introduction

Hepatocellular carcinoma (HCC) is the fifth most frequent malignant neoplasm worldwide and, owing to the lack of effective treatment options, is the third leading cause of cancer-related mortality [1]. HCC is often diagnosed at an advanced stage when it is no longer amenable to curative therapies. Alterations in the endogenous tumor suppressor networks seem to contribute to the resistance of HCC to classic cancer chemotherapies because the activity of most conventional chemotherapeutic agents highly depends on innate pro-apoptotic pathways that are disabled in HCC [2]. Other mechanisms of chemotherapy resistance of cancers are related to the tumor microenvironment [3].

The efficacy of drugs against solid tumors such as HCC is limited by resistance and toxicity resulting from the action on nontumor cells. Therefore, large efforts are under way to identify molecules, the inhibition of which preferentially kills malignant cells. The mitosis-associated serine/threonine kinase Polo-like kinase 1 (Plk1) is a good candidate to fulfill this condition [4]. Thus, most malignancies show higher Plk1 expression than their normal counterparts, and inhibition of Plk1 results in spindle dysfunction, mitotic checkpoint activation, G_2-M phase arrest, and apoptosis in cancer cells [4]. High Plk1 expression has also been reported in HCC, and the suppression of Plk1 expression by RNA interference (RNAi) reduced the proliferation of HCC cells [5–7], suggesting that Plk1 might be a suitable target in HCC. Interestingly, there is evidence that cancer cells might be more sensitive to Plk1 inhibition than primary nontransformed cells [8–13]. These results have prompted the development of Plk1-specific small-molecule inhibitors, some of which are currently in clinical trials [14]. Plk1 inhibitors such as BI 2536 show high efficacy in cultured tumor cells and nude mice tumor xenografts. However, clinical trials in patients with different tumor entities revealed only modest clinical efficacy, hematotoxicity being dose-limiting [14]. Obviously, these preclinical tumor models do not faithfully predict or recapitulate the clinical efficacy of the Plk1 inhibitor.

In genetically engineered mouse (GEM) tumor models, the spontaneous and unconstrained way in which such tumors evolve well reflects both the tumor cell and microenvironmental features of naturally occurring cancers [15–17]. GEM tumor models may better predict therapy outcome compared with nude mice bearing transplanted tumors has been provided for pancreatic ductal carcinoma and non–small cell lung cancer [18,19], but this has not yet been examined for HCC, and GEM tumor models have not yet been used to examine Plk1-directed therapeutics. To investigate if Plk1 indeed might be a suitable target in HCC and to explore if a GEM HCC model are suitable to study anti-Plk1 therapy, we here compared the therapeutic efficacy of Plk1 inhibition by RNAi as well as the Plk1 inhibitor BI 2536 in cultured HCC cells, nude mice xenografted with HCC, and in a transgenic mouse model (transforming growth factor (TGF)α/c-myc) developing HCC endogenously. Our data support the contention that Plk1 is a highly promising target in HCC and that TGFα/c-myc mice are suitable to study anti-HCC therapy. The Plk1 inhibitor BI 2536 inhibited hepatocarcinogenesis but was ineffective in HCC in TGFα/c-myc mice. Measurement of BI 2536 concentrations revealed much lower levels in the tumors compared with the normal liver tissue, which may explain the lack of efficacy of BI 2536 in HCC of TGFα/c-myc mice. Thus, insufficient drug levels might be a mechanism of primary resistance in HCC.

Materials and Methods

Cell Culture

Huh-7 cells (kindly provided by K. Breuhahn, University of Heidelberg) were grown in RPMI 1640 medium supplemented with 10% fetal calf serum and penicillin/streptomycin (Invitrogen, Carlsbad, CA).

Nude Mice Experiments

All animal experiments were approved by the local Animal Care Committee and were in agreement with German legal requirements. A total of 8×10^6 Huh-7 cells (resuspended in 150 μl of phosphate-buffered saline [PBS]) were injected subcutaneously into the flanks of CD1 nude mice (Charles River, Wilmington, MA). When the tumors reached a diameter of 2 to 3 mm, 7×10^9 plaque-forming units (pfu) of adenoviral suspensions (AdV control or AdV-Plk1) were slowly injected into the tail vein. Each treatment group consisted of seven mice. Body weight and tumor size were determined every 3 days. At the end of the experiment, the mice were sacrificed by cervical dislocation. Tumors were excised, weighed, and snap frozen at –80°C until further use.

To study the effect of BI 2536 (kindly provided by Boehringer Ingelheim, Vienna, Austria, or was purchased from Axon, Groningen, the Netherlands) on Huh-7 xenograft progression in nude mice, animals with established tumors received 30 mg/kg BI 2536 twice per week. Body mass and tumor size were measured and recorded.

To determine the rate of infection of the Huh-7 tumors with intravenously administered AdV, mice harboring 2 to 3 mm tumors received 7×10^9 pfu of AdV-LacZ or AdV control. After 72 hours, the tumors were excised and 7-μm-thick cryosections were produced. The sections were fixed in fixative solution (0.5% glutaraldehyde in $MgCl_2$-PBS solution) for 20 minutes. Subsequently, the sections were rinsed twice in PBS and incubated in 5-bromo-4-chloro-3-indolyl-β-D-galactopyranoside (X-Gal) staining solution (InvivoGen, San Diego, CA) for 45 minutes at 37°C, followed by rinsing four times with PBS. Counterstaining was performed with Nuclear Fast Red (0.1% in 5% $Al_2(SO_4)_3$) (Sigma-Aldrich, St. Louis, MO).

Transgenic Mice Experiments

Male TGFα/c-myc bitransgenic mice were produced by crossing homozygous metallothionein/TGFα and albumin/c-myc single transgenic mice in CD13B6CBA background as described [20,21]. To minimize bias from interindividual variation, littermates were assigned to the two treatment groups. Directly after weaning, the mice received $ZnCl_2$ to induce the expression of TGFα and thereby accelerate hepatocarcinogenesis. The body weights were recorded during the treatments. To study the effect of BI 2536 on hepatocarcinogenesis, the mice received either BI 2536 (30 mg/kg) or PBS intravenously twice weekly from week 12 to 16 after beginning of the zinc induction. The whole livers from the TGFα/c-myc mice were fixed in 4% neutral formalin at 4°C overnight. Pieces of 1 to 1.5 g of liver were examined histopathologically.

To study the effect of BI 2536 on HCC progression, TGFα/c-myc mice were induced with $ZnCl_2$ for 20 to 23 weeks. To detect and monitor the endogenously formed HCCs in the TGFα/c-myc mice, contrast-enhanced magnetic resonance imaging (MRI) using gadoxetic acid contrast agent (Primovist, Bayer-Schering, Berlin, Germany) and a 3-T MRI scanner (Siemens Magnetom Trio, Siemens Medical Solutions, Erlangen, Germany). Before imaging, animals were anesthetized

using ketamine (70 mg/kg) and xylazine (12 mg/kg), injected with gadoxetic acid (0.057 mmol/kg), and positioned in the scanner. The imaging sequences included T1-weighted sequences with following parameters: echo time = 20 milliseconds, repetition time = 947 milliseconds, field of view = 100 mm, slice thickness = 1 mm, flip angle = 140°, fat suppression = fat saturated. All animals were imaged in the axial plane.

Two weeks after the first tumor detection, mice received another MRI and tumor progression was determined. Mice with verified tumors received 30 mg/kg BI 2536 twice per week for 4 weeks. At the end of treatment, the tumor size was again measured by MRI.

All analytic procedures and additional methods are described in the Supplementary Materials and Methods.

Results

Validation of Plk1 as Target in HCC

Plk1 is a promising target for cancer therapy [4]. Small-molecule Plk1 inhibitors are currently examined for their efficacy in several cancer entities, but the feasibility of using small-molecule inhibitors for HCC has not yet been investigated. We initially confirmed recent findings [5–7] that most HCC express considerably higher levels of Plk1 at the mRNA and protein levels compared with the surrounding normal liver tissue (Figure W1).

To investigate whether Plk1 inhibition might be an effective strategy to inhibit HCC, we studied the effect of BI 2536 as well as of an adenoviral vector driving the expression of an optimized short hairpin (sh)RNA against Plk1 (AdV-Plk1) on the viability of HCC cell lines. BI 2536 as well as AdV-Plk1, but not an adenovirus encoding a control short hairpin RNA (shRNA) (AdV control), reduced the viability and increased apoptosis of Huh-7 cells (Figure 1, A, B, E, and F). We confirmed that AdV-Plk1, but not AdV control, decreased Plk1 expression (Figure W2). Similar data were obtained in three other HCC cell lines (HepG2, Hep3B, and PLC/PRF/5; data not shown). We also checked if BI 2536 and AdV-Plk1 elicit the characteristic effects of Plk1 inhibition, that is, mitotic G_2-M phase arrest and monoastral spindles in Huh-7 cells by fluorescence-activated cell sorting (FACS) and immunocytochemical analyses. Indeed, BI 2536 as well as AdV-Plk1, but not AdV control, strongly increased the amount of cells with 4N and elicited monoastral spindles (Figure 1, C, D, G, and H).

Next we studied the effects of BI 2536, AdV-Plk1, and AdV control on the progression of Huh-7 xenografts in nude mice. To this end, BI 2536 or PBS was injected intravenously into nude mice bearing Huh-7 cell tumors twice weekly. The size of the tumors was measured 4, 7, and

11 days after the beginning of treatment. As illustrated in Figure 2A, treatment of nude mice bearing Huh-7 xenografts with BI 2536 clearly inhibited the progression of the xenografts ($P < .05$).

To investigate the effect of RNAi-induced suppression of Plk1 expression on the progression of Huh-7 xenografts in nude mice, we first determined the ability of systemically administered AdV to effectively infect Huh-7 xenografts in nude mice. AdV-LacZ or vehicle as a control was injected intravenously into Huh-7 tumor-bearing nude mice. Three days later, the tumors were excised and 50 histologic sections were examined for the presence of β-galactosidase by X-Gal staining. About 10% to 70% of the tumor cells from AdV-LacZ–treated animal showed positive X-Gal staining (Figure W3, *middle and right panels*). The tumors of saline-injected animals were analyzed and found not to contain positive X-Gal–stained cells (Figure W3, *left panel*). These data indicated that the Huh-7 tumors in the nude mice were infected to a considerable extent on intravenous administration of AdVs.

We next evaluated whether systemic administration of AdV-Plk1 reduced HCC tumor progression in the Huh-7 xenograft mouse model. To this end, AdV-Plk1, AdV control or PBS were injected once intravenously into nude mice bearing Huh-7 cell tumors (as performed above with AdV-LacZ). The size of the tumors was measured every 3 days for a period of 1 month. The tumors in AdV-Plk1–treated mice grew slower than tumors in AdV control–treated animals, whereas AdV control had no significant effect (Figure 2B), verifying that the growth inhibitory effect of AdV-Plk1 was specific for the Plk1-shRNA encoded by the AdV and not by the AdV infection itself.

To investigate if the inhibitory effect of AdV-Plk1 on HCC tumor progression was due to Plk1 depletion, Huh-7 tumors were excised 3, 4, 7, or 14 days after injection of the virus into the mice and analyzed for Plk1 expression by immunoblot analysis. As shown in Figure 2C, the Plk1 levels were reduced in tumors from AdV-Plk1–treated mice compared with animals that received the control virus. Reduced Plk1 protein expression was detectable up to 7 days after administration of the AdV to the animals, whereas 14 days after injection, down-modulation of Plk1 expression was not detectable any more. Analyses of the tumor extracts for an apoptotic marker (cleaved poly[ADP-ribose] polymerase [PARP]) by immunoblot analysis revealed the emergence of cleaved PARP fragment in tumor extracts from AdV-Plk1–treated mice, but not in tumors from AdV control–treated animals (Figure 2C), suggesting that AdV-Plk1, but not AdV control increased the rate of apoptosis in the HCC tumors. Together, these data indicate that inhibition of Plk1 activity by BI 2536 or suppression of Plk1 expression by RNAi caused similar anti-HCC effects in cultured HCC cell lines and Huh-7 xenografts.

Figure 1. BI 2536 as well as AdV-Plk1 decreased the viability of cultured Huh-7 cells. (A, B) BI 2536 dose-dependently decreased the viability of Huh-7 cells. Huh-7 cells were exposed to the indicated concentration of BI 2536. After 48 hours, the viable cell mass was analyzed by the MTT test (A), the amount of apoptotic cells was detected after 24 hours by Hoechst staining (B). Bars signify means ± SD of duplicates. For each condition, at least 1400 cells were evaluated. (C) BI 2536 elicited G_2-M arrest. Huh-7 cells were exposed to BI 2536 for 30 hours, followed by FACScan analysis. Cells with subgenomic DNA content were not gated. (D) BI 2536–treated Huh-7 cells show monoastral spindles. The cells were treated with BI 2536 (10 nM) for 2 days and stained for α-tubulin and DNA. (E, F) AdV-Plk1 reduced the viability of Huh-7 cells. The cells were infected with 10^5 pfu/ml of AdV-Plk1 or AdV control. After the indicated time, the viable cell mass was analyzed by the MTT test (E). (F) AdV-Plk1 increased the amount of apoptotic cells, whereas AdV control did not. At 24 hours after treatment with AdV-Plk1 or AdV control, the number of apoptotic cells was determined. Bars signify means ± SD of five independent determinations. The values were significantly different between AdV control and AdV-Plk1–treated cells (*$P > .05$). (G) FACScan analysis of Huh-7 cells performed 30 hours after infection with AdV-Plk1, AdV control, or no treatment. Cells with subgenomic DNA content were not gated. AdV-Plk1, but not AdV control, elicited an increase in the amount of cells with 4N. (H) Phenotype of Huh-7 cells treated with AdV-Plk1 (10^5 pfu/ml). α-Tubulin immunostaining is shown in red; DNA is shown in cyan. AdV-Plk1 treatment elicited monoastral spindles.
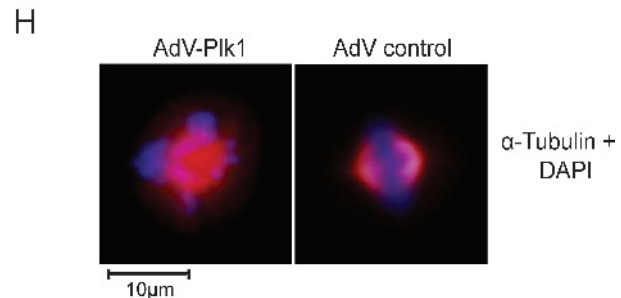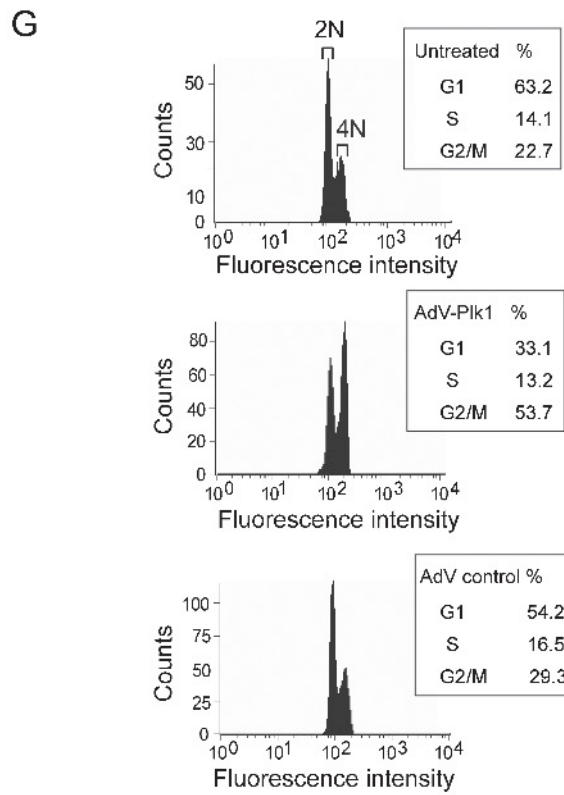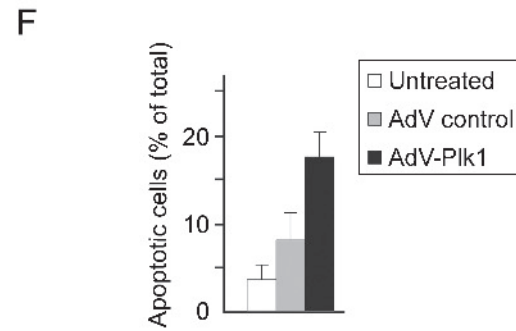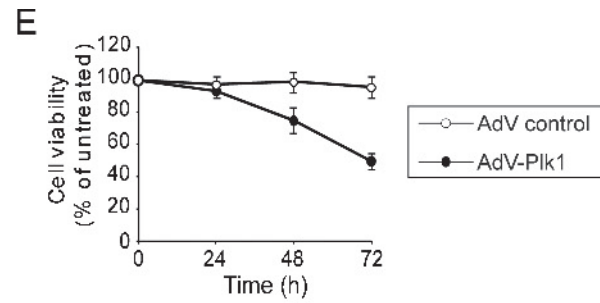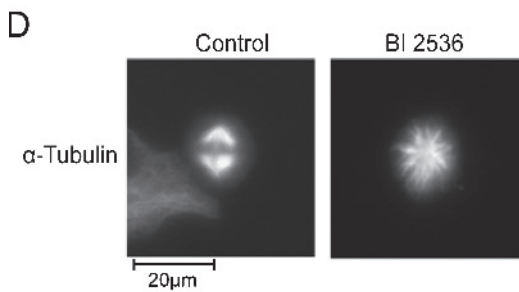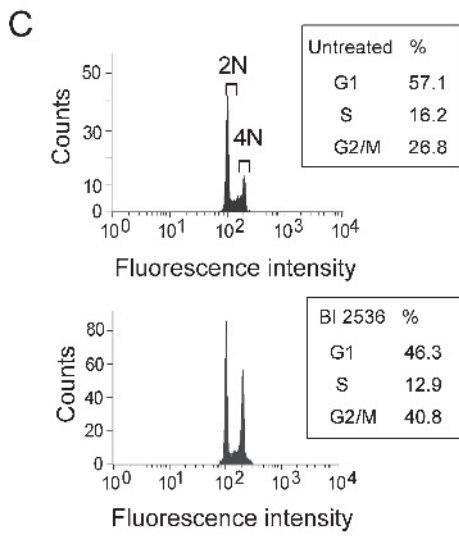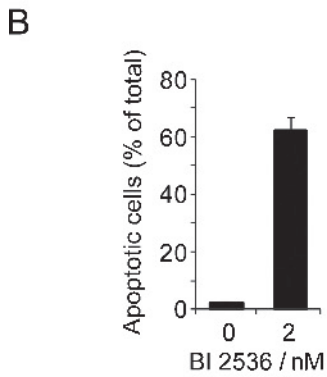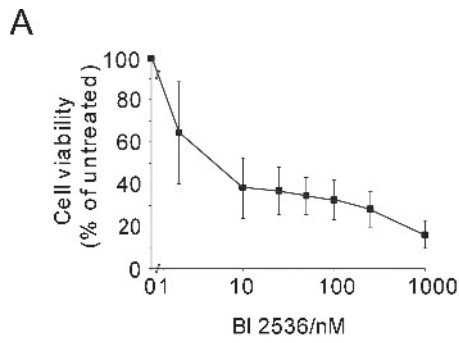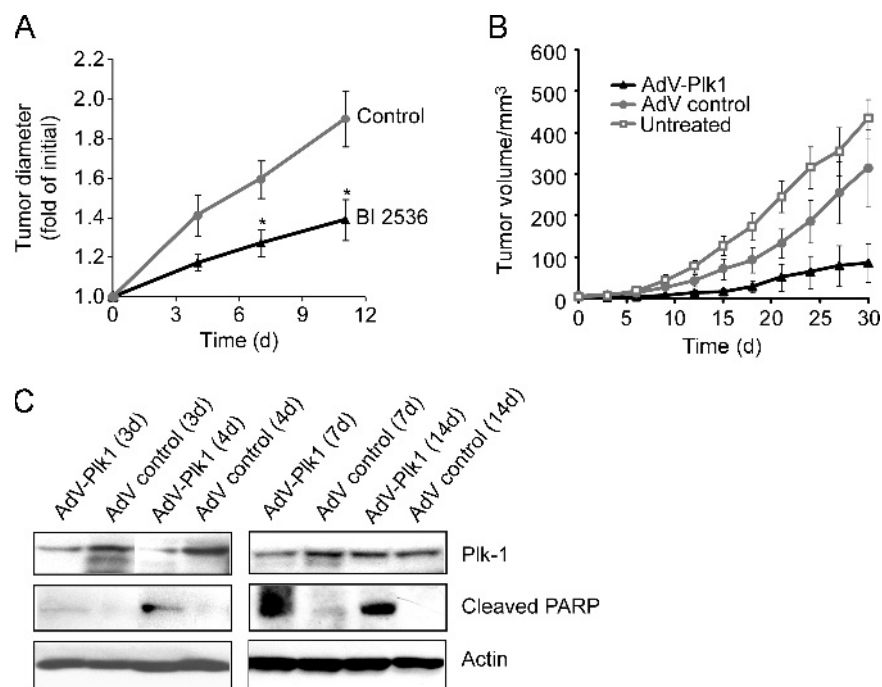
Figure 2. BI 2536 as well as AdV-Plk1 suppressed Huh-7 tumor progression in nude mice. When the tumors reached a diameter of 2 to 3 mm, 300 μl (7 × 10⁹ pfu) of AdV-Plk1 (encoding a shRNA against Plk1), AdV control suspension, or saline was injected intravenously into nude mice. (A) BI 2536 reduced Huh-7 tumor xenograft progression in nude mice. When the tumors reached a diameter of 2 to 3 mm, BI 2536 (30 mg/kg) or saline was injected intravenously twice per week. Error bars represent the standard error of the mean. Asterisks indicate a significant difference between the tumor diameters of BI 2536– or saline-treated animals ($P < .05$). (B) Growth curves of Huh-7 tumors after no treatment or intravenous application of AdV-Plk1 or AdV control revealed that AdV-Plk1 but not AdV control reduced tumor progression. The differences in tumor volume between mice treated with AdV control or AdV-Plk1 were significant ($P < .05$) from day 3 after the treatment. Error bars represent the SD. (C) Down-regulation of Plk1 levels and occurrence of cleaved PARP fragment in subcutaneous Huh-7 tumors from mice treated with AdV-Plk1. After the indicated duration postinjection of AdV control or AdV-Plk1, tumors were excised and analyzed by anti-Plk1, anti-PARP, and anti–β-actin immunoblot analysis.

BI 2536 Has No Significant Effect on HCC Progression in TGFα/c-myc Mice

Because of the limited predictability of cell culture and tumor xenograft models for clinical efficacy, including tumor xenograft models for Plk1-targeting therapeutics, and the evidence for superiority of certain GEM to nude mice tumor models with respect to predicting clinical outcome in other cancer entities, we investigated Plk1 targeted therapy in the TGFα/c-myc–driven HCC mouse model. Aberrant expressions of c-myc as well as TGFα are frequent in primary human HCCs [22–24], and the TGFα/c-myc–driven hepatocarcinogenesis models quite closely resemble various histopathologic, biochemical, and cytogenetic features characteristic of human liver oncogenesis [21]. Therefore, we tested the effect of BI 2536, which also inhibits the activity of mouse Plk1 [25], on HCC progression in TGFα/c-myc mice. Primovist-enhanced MRI was used to detect the endogenous HCCs in TGFα/c-myc mice. HCCs were detectable 16 to 20 weeks after beginning of the induction of the hepatocarcinogenesis. HCC progression before the treatment was determined by two MRI measurements separated by 2 weeks. After the second MRI, mice were either treated with BI 2536 (30 mg/kg) or saline twice weekly for 4 weeks. After the end of the treatment, the animals received a further MRI to determine posttreatment size of HCC. BI 2536 treatment tended to reduce HCC progression in TGFα/c-myc mice, but this did not reach statistical significance (Figure 3, A and B). After the last MRI, the animals were killed and radiologically detected HCCs were

confirmed by macroscopic inspection as well as histopathologically. BI 2536 had no significant effect on the body mass, hepatomegaly, cellular and nuclear enlargement, and nuclear atypia, all of which are characteristic of fast-growing TGFα/c-myc livers. Markers of liver function such as alanine aminotransferase and aspartate aminotransferase were enhanced in the transgenic mice compared with an age-matched control as reported earlier [26] but showed no significant changes on BI 2536 treatment (data not shown).

BI 2536 Reduces Hepatocarcinogenesis in TGFα/c-myc Mice

To investigate if BI 2536 inhibits hepatocarcinogenesis in TGFα/c-myc mice, double transgenic animals, in which hepatocarcinogenesis had been induced for 12 weeks, were injected with BI 2536 (30 mg/kg) twice weekly intravenously until week 16. BI 2536 treatment remarkably suppressed the tumorigenesis in TGFα/c-myc mice. All vehicle-treated mice had foci of altered hepatocytes in the liver and 25% of the vehicle-treated mice had dysplastic nodules (Table 1). Of the eight BI 2536–treated mice, two were devoid of preneoplastic foci (Table 1). In the BI 2536 treatment group, the number of foci per liver was half of that in the control group (6.9 ± 2.1 compared with 13.9 ± 1.7, $P < .05$), and the mean maximum focus diameter was 26% smaller (0.92 ± 0.27 compared with 1.25 ± 0.13, $P < .05$; Table 1). The expression of the proliferation marker Ki-67 was positive in seven of eight animals within the foci of vehicle-treated animals, whereas only one of eight of the BI 2536–treated animals contained a Ki-67–positive focus in the liver
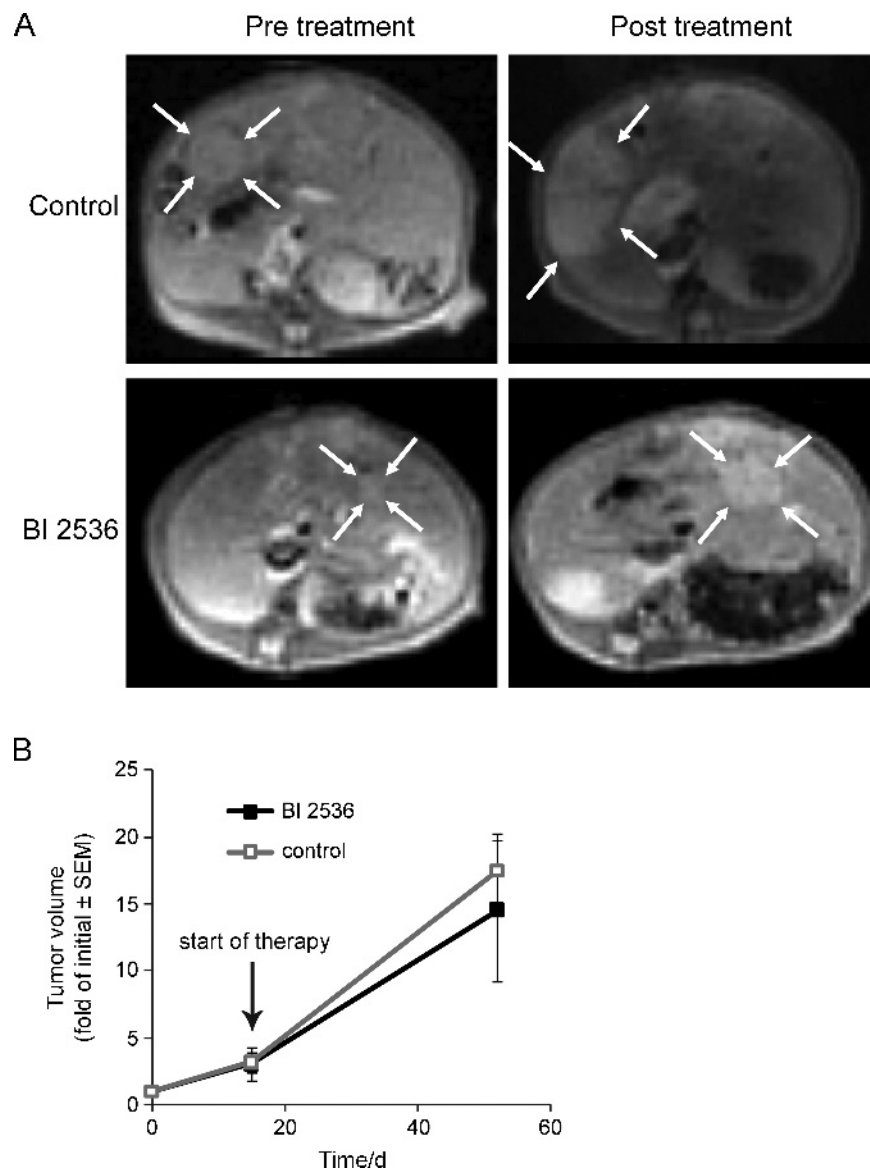
Figure 3. Effect of BI 2536 on HCC progression in TGFα/c-myc mice determined by MRI. TGFα/c-myc mice with HCC received two MRI separated by 2 weeks before the treatment. After the second MRI, the mice were either treated with BI 2536 (30 mg/kg) or saline twice weekly for 4 weeks. At the end of the treatment, the animals received a third MRI. (A) Pretreatment and end-of-treatment MRI examinations of a representative control (top) and a BI 2536–treated (bottom) HCC-bearing TGFα/c-myc mouse. TGFα/c-myc mice with HCC were treated twice per week with vehicle or BI 2536 (30 mg/kg) by intravenous injection after the second MRI. Index lesions are indicated by the arrows. (B) Quantitative analyses of the progression of HCC index lesions in BI 2536–treated (n = 5) and control animals (n = 5). Shown are means ± standard error of the mean. There were no significant differences between the two groups.

Table 1. Effect of BI 2536 on Hepatocarcinogenesis in TGFα/c-myc Mice.

Treatment Group	Incidence, %		No. Foci/Liver, Means ± SE	Mean Maximum Focus Diameter ± SE, mm
	Preneoplastic Foci	Dysplastic Nodules		
Vehicle	100 (8/8)*	25 (2/8)	13.9 ± 1.7	1.25 ± 0.13
BI 2536	75 (6/8)	0 (0/8)	6.9 ± 2.1	0.92 ± 0.27
P	NS	NS	.03	.026

The P value was calculated using Student t test for unpaired values. BI 2536 treatment of the animals reduced the number of foci per liver and the mean maximum focus diameter.
NS indicates not significant.
*The number of mice with preneoplastic foci/dysplastic nodules per total number of mice is shown in parentheses.
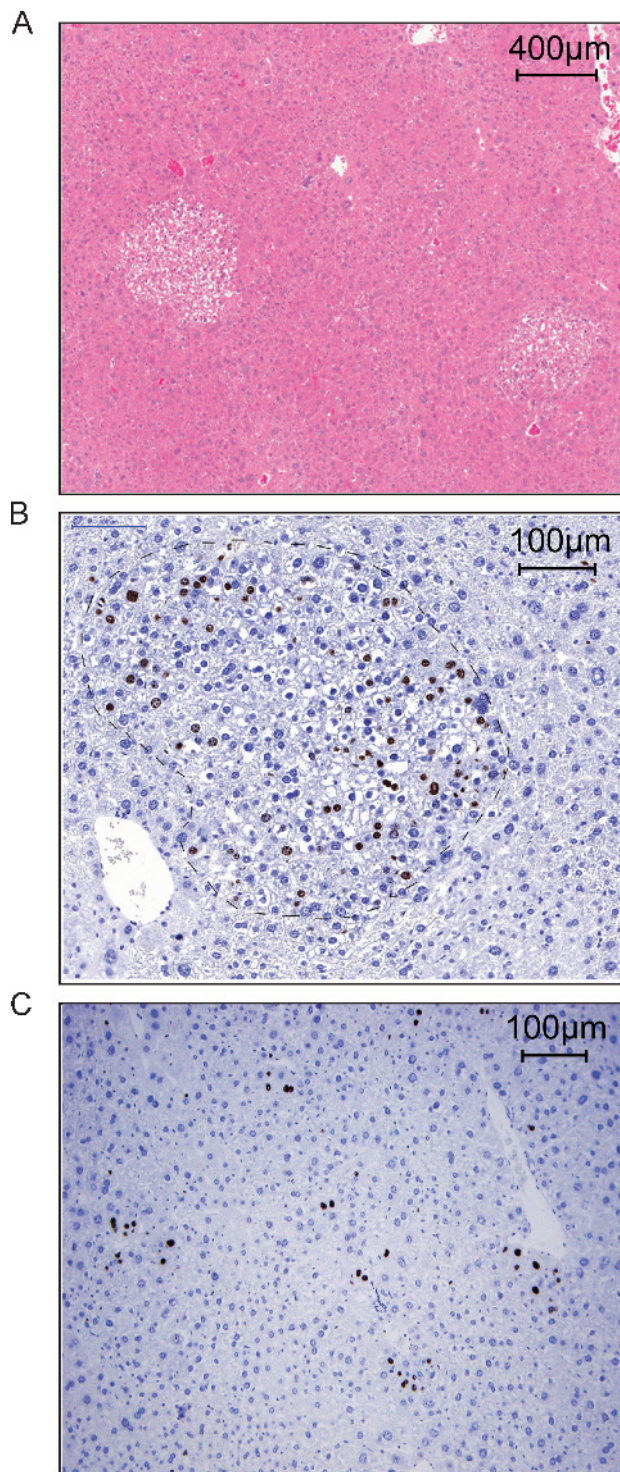
Figure 4. BI 2536 reduces Ki-67 expression in the foci of altered hepatocytes of livers of TGFα/*c-myc* mice. Male littermates of TGFα/c-*myc* mice were assigned to the two treatment groups. The animals received either BI 2536 (30 mg/kg) or PBS intravenously twice weekly from week 12 to 16 after beginning of the zinc induction, followed by sacrificing of the animals, removal of the livers, fixation of the livers in formalin, and sectioning. (A) Hematoxylin-eosin staining. (B) Ki-67 staining of liver sections from vehicle-treated TGFα/*c-myc* mouse revealed Ki-67–positive hepatocytes within a focus of altered hepatocytes. The focus is within the light dashed line. (C) Ki-67 staining of liver sections from BI 2536–treated TGFα/ *c-myc* mouse occasionally revealed Ki-67–positive hepatocytes with no relation to foci of altered hepatocytes.

Table 2. Effect of BI 2536 on Ki-67 Expression in the Livers of TGFα/*c-myc* Mice.

Treatment Group	Incidence, %	
	Ki-67 Negative or without Relation to Foci	Ki-67 Expression within Foci or Nodules
Vehicle	25 (2/8)*	75 (6/8)
BI 2536	87.5 (7/8)	12.5 (1/8)
P	<.05	<.05

The *P* value was calculated using the Fisher exact test. BI 2536 treatment of the animals increased the number of Ki-67–negative foci and foci-positive for Ki-67 but without relation to the foci.
*The number of mice with preneoplastic foci/dysplastic nodules per total number of mice is shown in parentheses.

(Figure 4, *A* and *B*, and Table 2). Four of eight BI 2536–treated animals contained Ki-67–positive cells with no relation to preneoplastic foci (Figure 4*C* and Table 2). These data indicated that BI 2536 suppressed hepatocarcinogenesis in TGFα/*c-myc* mice.

Reduced Levels of BI 2536 in HCC Tissue Compared to Normal Liver Tissue

Recent evidence from other cancer entities suggests that insufficient intratumoral drug levels might be an important cause of lack of therapeutic efficacy [18]. To investigate if insufficient intratumoral levels of BI 2536 could be a reason for the lack of effect of BI 2536 on the HCC in TGFα/*c-myc* mice, mice were injected intravenously with BI 2536 (30 mg/kg) and the concentration of BI 2536 was determined in HCC as well as normal liver tissue at various time points after the injection by mass spectrometry. As illustrated in Figure 5*A*, the concentration of BI 2536 was lower in the tumor than in the normal liver tissue. Twelve hours after the injection, the concentration of BI 2536 in tumor was only 20% of that in the normal liver tissue (Figure 5*B*).

Reduced Perfusion of Tumors Compared to Normal Liver Tissue in TGFα/c-myc Mice

To investigate if the reduced the levels of BI 2536 in HCC compared with adjacent normal liver tissue in TGFα/*c-myc* mice might be due to lower drug delivery, we studied the perfusion of HCC and adjacent normal liver tissue by contrast-enhanced MRI using the intravascular contrast agent Glowing Galbumin-Rhodamine B. As illustrated in Figure W4, *A* and *B*, contrast enhancement elicited by Glowing Galbumine-Rhodamine B in HCC tissue ranged between 0.33- and 0.96-fold of the contrast enhancement in normal liver tissue (mean value = 0.66 ± 0.24, *P* < .05 according to 1-tailed Student's *t* test). Analysis of cryosections of the livers by confocal laser scanning microscopy revealed higher fluorescence signals in normal liver tissue compared with tumor tissue (Figure W4*C*). These data indicate that HCC shows lower blood perfusion compared with normal liver tissue in TGFα/*c-myc* mice.

Discussion

The development of more effective therapies against solid tumors such as HCC is likely to profit from the identification of targets, the inhibition of which preferentially kills malignant cells. Plk1 is a good candidate to fulfill this condition [4]. Indeed, targeting Plk1 using both *in vivo* small interfering RNA delivery systems and novel small-molecule inhibitors elicits significant reduction of the growth of cultured tumor cells as well as of tumor progression in a number of transplanted tumor models [8–12,25,27–34]. Moreover, although
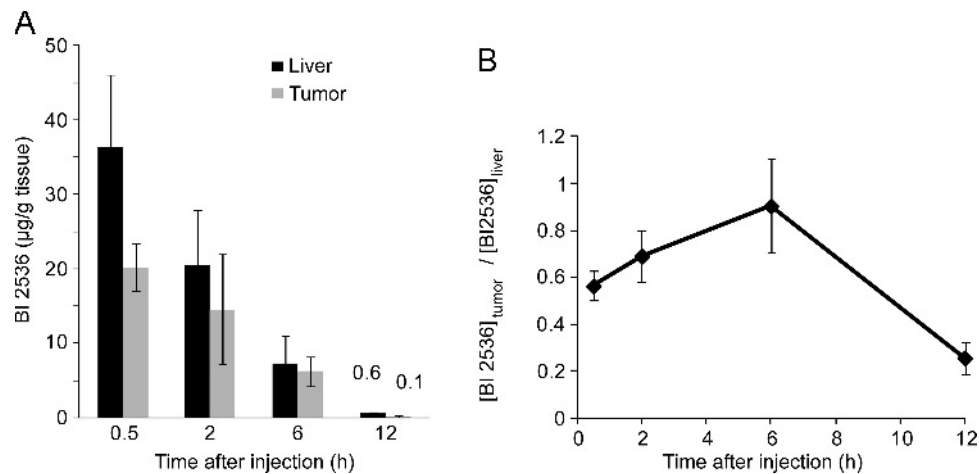
Figure 5. Reduced levels of BI 2536 in HCC of TGFα/*c-myc* mice. TGFα/*c-myc* mice bearing HCC (two per time point) were injected intravenously with BI 2536 (30 mg/kg). After the indicated time, the mice were sacrificed, the liver was excised, and tissue samples of HCC and non-HCC tissue were obtained. The amount of BI 2536 was determined in HCC as well as normal liver tissue at various time points by mass spectrometry. (A) Levels of BI 2536 in liver and tumor tissue at different time. Bars signify means ± SD of samples from two animals. (B) Ratio of BI 2536 content in tumor tissue to that in liver tissue. Values are means ± SD.

complete loss of Plk1 is incompatible with cell division [35], there is evidence that nontransformed cells require less Plk1 than tumor cells [8–13], and Plk1 came up in synthetic lethal screens [36], rendering Plk1 a highly interesting target in cancer. Despite these promising preclinical data, the first clinical results with Plk1 inhibitors, including BI 2536, in patients with various solid cancers were disappointing [36]. Obviously, the preclinical tumor models do not appropriately model the human therapeutic situation. Therefore, it is important to identify tumor models that are more predictive for clinical success and may allow the identification of the mechanisms of resistance. Comparative studies for the efficacy of chemotherapeutics in transgenic and transplanted cancer models have been performed in K-*ras*–driven models of pancreatic ductal adenocarcinoma and non–small cell lung cancer and indicate that these transgenic tumor models may better reflect the therapeutic efficacy of standard therapeutics in patients with the corresponding malignant diseases than the nude mice models [17–19].

In the present study, we examined the efficacy of inhibition of Plk1 for anti-HCC therapy using different HCC models. Our data indicate that Plk1 is a promising therapeutic target in HCC, but the therapeutic efficacy of the Plk1 inhibitor BI 2536 is compromised by low intratumoral drug levels. We found much stronger Plk1 expression in HCC compared with normal liver tissue from the same patient and that Plk1 inhibition by RNAi as well as the Plk1 inhibitor BI 2536 effectively inhibited HCC progression in cultured HCC cells or nude mice xenografted with HCC. In contrast, there was no significant effect of BI 2536 on HCC progression in the transgenic HCC mouse model. Our finding that BI 2536 inhibited hepatocarcinogenesis indicates that insufficient systemic drug levels were unlikely to be causative for its failure to reduce progression of manifest HCC in the transgenic mouse model. The sensitivity of the transgenic HCC model to BI 2536 paralleled the limited therapeutic efficacy of these Plk1 inhibitors in early clinical studies in patients with different malignancies [14,37]. Thus, it seems likely that the effect of BI 2536 in TGFα/*c-myc* HCC mice may better reflect the clinical efficacy of BI 2536 and potentially other Plk1 inhibitors in HCC patients compared to nude mice bearing HCC xenografts, although results with BI 2536 in HCC patients are still lacking.

There is growing evidence that the tumor microenvironment plays a crucial role in chemotherapy resistance [38] and that GEM tumor models better reflect the impact of the tumor microenvironment on chemotherapy resistance than transplanted tumor models. Thus, in a GEM of ductal pancreatic cancer, the endogenous tumors are resistant to gemcitabine, whereas the isolated cancer cells or transplants of these cells were drug sensitive [18], indicating that the tumor stroma confers chemotherapy resistance in this tumor model. Transplanted tumors often lack the stromal organization and adaptation to host immune defense that occur in tumors that arise because a slow process of progressive genetic and epigenetic changes [39,40]. A complex signaling cross talk between the different cell types in the tumor stroma and the cancer cells themselves as well as the increased interstitial fluid pressure in the tumors may contribute to the chemotherapy resistance of malignant tumors [3,18,38,41]. Recent data suggest that bone marrow microenvironment confers resistance to BI 2536 in a model of multiple myeloma [42]. The present study shows that, on intravenous injection of BI 2536, the concentration of the drug is considerably lower in the HCCs than in the surrounding normal liver tissue, representing a not-yet-recognized mechanism for resistance to BI 2536. Thus, it is possible that low intratumoral drug levels contribute to the rather limited clinical efficacy of BI 2536 observed in a number of other malignancies. An important consequence is that the limited clinical antitumor efficacy of BI 2536 and perhaps other Plk1 inhibitors reported up to now does not mean that Plk1 is an unsuitable target. If higher intratumoral drug levels can be achieved, Plk1 might be a highly promising potentially tumor-selective target in HCC and other malignant diseases.

The data of the present study indicate that insufficient drug delivery might be causative for the low intratumoral drug levels, because Galbumin-enhanced MRI as well as by confocal laser scanning fluorescence microscopy indicated lower blood perfusion in tumor tissue compared with the normal liver tissue. Lower blood perfusion of tumor compared with normal tissue has also been reported in other cancer models [18,43].

A recent study has shown that inhibition of Plk1 suppresses hepatitis B virus X protein–induced transformation in an *in vitro* model

of liver cancer progression [44] and that Plk1 expression is upregulated in chemically induced hepatocarcinogenesis [45]. In the present study, BI 2536 inhibited hepatocarcinogenesis in the TGFα/*c-myc* mice, whereas established HCCs show only slight if any response to this compound. In particular, we found that the number of preneoplastic foci was considerably reduced in livers of BI 2536–treated TGFα/*c-myc* mice and contained less Ki-67–positive cells. BI 2536 had no significant influence on other characteristics of the fast-proliferating TGFα/*c-myc* livers, including hepatomegaly, cellular and nuclear enlargement and atypia, suggesting that Plk1 inhibition did not reduce the increased rate of proliferation owing to the presence of the transgene. Thus, it seems possible that hepatocyte regeneration required to maintain liver function in patients with liver cirrhosis might be less compromised by BI 2536 than hepatocarcinogenesis. Moreover, because some naturally occurring compounds inhibit Plk1 activity, a nontoxic Plk1 inhibitor might be used for HCC chemoprevention in patients with chronic hepatitis bearing a high risk to develop HCC.

In summary, our study shows that Plk1 is a promising target in HCC and indicate that low intratumoral drug levels rather than unsuitability of Plk1 as drug target may account for the low clinical efficacy of BI 2536 and possibly other Plk1 inhibitors. Thus, the efficacy of anti-Plk1 therapy with BI 2536 might be considerably increased on elevation of the reduced BI 2536 levels.

Acknowledgments

References

[1] Llovet JM and Bruix J (2008). Molecular targeted therapies in hepatocellular carcinoma. *Hepatology* **48**, 1312–1327.

[2] Lowe SW, Cepero E, and Evan G (2004). Intrinsic tumour suppression. *Nature* **432**, 307–315.

[3] Östman A and Augsten M (2009). Cancer-associated fibroblasts and tumor growth—bystanders turning into key players. *Curr Opin Genet Dev* **19**, 67–73.

[4] Strebhardt K (2010). Multifaceted Polo-like kinases: drug targets and antitargets for cancer therapy. *Nat Rev Drug Discov* **9**, 643–660.

[5] Bassermann F, Frescas D, Guardavaccaro D, Busino L, Peschiaroli A, and Pagano M (2008). The Cdc14B-Cdh1-Plk1 axis controls the G$_2$ DNA-damage-response checkpoint. *Cell* **134**, 256–267.

[6] He Z, Zheng H, Lin H, Miao XY, and Zhong DW (2009). Overexpression of Polo-like kinase 1 predicts a poor prognosis in hepatocellular carcinoma patients. *World J Gastroenterol* **15**, 4177–4182.

[7] Pellegrino R, Calvisi DF, and Ladu S (2010). Oncogenic and tumor suppressive roles of Polo-like kinases in human hepatocellular carcinoma. *Hepatology* **51**, 857–868.

[8] Elez R, Piiper A, Giannini CD, Brendel M, and Zeuzem S (2000). Polo-like kinase 1, a new target for antisense tumor therapy. *Biochem Biophys Res Commun* **269**, 352–356.

[9] Elez R, Piiper A, Kronenberger B, Kock M, Brendel M, Hermann E, Pliquett U, Neumann E, and Zeuzem S (2003). Tumor regression by combination antisense therapy against Plk1 and Bcl-2. *Oncogene* **22**, 69–80.

[10] Guan R, Tapang P, Leverson JD, Albert D, Giranda VL, and Luo Y (2005). Small interfering RNA-mediated Polo-like kinase 1 depletion preferentially reduces the survival of p53-defective, oncogenic transformed cells and inhibits tumor growth in animals. *Cancer Res* **65**, 2698–2704.

[11] Gumireddy K, Reddy MV, Cosenza SC, Boominathan R, Baker SJ, Papathi N, Jiang J, Holland J, and Reddy EP (2005). ON01910, a non–ATP-competitive small molecule inhibitor of Plk1, is a potent anticancer agent. *Cancer Cell* **7**, 275–286.

[12] Liu X, Lei M, and Erikson RL (2006). Normal cells, but not cancer cells, survive severe Plk1 depletion. *Mol Cell Biol* **26**, 2093–2108.

[13] Raab M, Kappel S, Krämer A, Sanhaji M, Matthess Y, Kurunci-Csacsko E, Calzada-Wack J, Rathkolb B, Rozman J, Adler T, et al. (2011). Toxicity modelling of Plk1-targeted therapies in genetically engineered mice and cultured primary mammalian cells. *Nat Commun* **2**, 395.

[14] Schöffski P (2009). Polo-like kinase (PLK) inhibitors in preclinical and early clinical development in oncology. *Oncologist* **14**, 559–570.

[15] Sharpless NE and Depinho RA (2006). The mighty mouse: genetically engineered mouse models in cancer drug development. *Nat Rev Drug Discov* **5**, 741–754.

[16] Teicher BA (2006). Tumor models for efficacy determination. *Mol Cancer Ther* **5**, 2435–2443.

[17] Mazur PK and Siveke JT (2011). Genetically engineered mouse models of pancreatic cancer: unravelling tumour biology and progressing translational oncology. *Gut*, Aug 26 [Epub ahead of print].

[18] Olive KP, Jacobetz MA, Davidson CJ, Gopinathan A, McIntyre D, Honess D, Madhu B, Goldgraben MA, Caldwell ME, Allard D, et al. (2009). Inhibition of Hedgehog signaling enhances delivery of chemotherapy in a mouse model of pancreatic cancer. *Science* **324**, 1457–1461.

[19] Singh M, Lima A, Molina R, Hamilton P, Clermont AC, Devasthali V, Thompson JD, Cheng JH, Bou Reslan H, Ho CC, et al. (2010). Assessing therapeutic responses in *Kras* mutant cancers using genetically engineered mouse models. *Nat Biotechnol* **28**, 585–593.

[20] Jhappan C, Stahle C, Harkins RN, Fausto N, Smith GH, and Merlino GT (1990). TGFα overexpression in transgenic mice induces liver neoplasia and abnormal development of the mammary gland and pancreas. *Cell* **61**, 1137–1146.

[21] Murakami H, Sanderson ND, Nagy P, Marino PA, Merlino G, and Thorgeirsson SS (1993). Transgenic mouse model for synergistic effects of nuclear oncogenes and growth factors in tumorigenesis: interaction of *c-myc* and transforming growth factor α in hepatic oncogenesis. *Cancer Res* **53**, 1719–1723.

[22] Yaswen P, Goyette M, Shank PR, and Fausto N (1985). Expression of c-Ki-*ras*, c-Ha-*ras*, and c-*myc* in specific cell types during hepatocarcinogenesis. *Mol Cell Biol* **5**, 780–786.

[23] Morimitsu Y, Hsia CC, Kojiro M, and Tabor E (1995). Nodules of less-differentiated tumor within or adjacent to hepatocellular carcinoma: relative expression of transforming growth factor-α and its receptor in the different areas of tumor. *Hum Pathol* **26**, 1126–1132.

[24] Kaposi-Novak P, Libbrecht L, Woo HG, Lee YH, Sears NC, Coulouarn C, Conner EA, Factor VM, Roskams T, and Thorgeirsson SS (2009). Central role of c-Myc during malignant conversion in human hepatocarcinogenesis. *Cancer Res* **69**, 2775–2782.

[25] Steegmaier M, Hoffmann M, Baum A, Lénárt P, Petronczki M, Krssák M, Gürtler U, Garin-Chesa P, Lieb S, Quant J, et al. (2007). BI 2536, a potent and selective inhibitor of Polo-like kinase 1, inhibits tumor growth *in vivo*. *Curr Biol* **17**, 316–322.

[26] Kao CY, Factor VM, and Thorgeirsson SS (1996). Reduced growth capacity of hepatocytes from c-myc and c-myc/TGF-α transgenic mice in primary culture. *Biochem Biophys Res Commun* **222**, 64–70.

[27] Peters U, Cherian J, Kim JH, Kwok BH, and Kapoor TM (2006). Probing cell-division phenotype space and Polo-like kinase function using small molecules. *Nat Chem Biol* **2**, 618–626.

[28] McInnes C, Mazumdar A, Mezna M, Meades C, Midgley C, Scaerou F, Carpenter L, Mackenzie M, Taylor P, Walkinshaw M, et al. (2006). Inhibitors of Polo-like kinase reveal roles in spindle-pole maintenance. *Nat Chem Biol* **2**, 608–617.

[29] Garland LL, Taylor C, Pilkington DL, Cohen JL, and Von Hoff DD (2006). A phase I pharmacokinetic study of HMN-214, a novel oral stilbene derivative with Polo-like kinase-1–interacting properties, in patients with advanced solid tumours. *Clin Cancer Res* **12**, 5182–5189.

[30] Lansing TJ, McConnell RT, Duckett DR, Spehar GM, Knick VB, Hassler DF, Noro N, Furuta M, Emmitte KA, Gilmer TM, et al. (2007). *In vitro* biological activity of a novel small-molecule inhibitor of Polo-like kinase1. *Mol Cancer Ther* **6**, 450–459.

[31] Santamaria A, Neef R, Eberspächer U, Eis K, Husemann M, Mumberg D, Prechtl S, Schulze V, Siemeister G, Wortmann L, et al. (2007). Use of the novel Plk1 inhibitor ZK-thiazolidinone to elucidate functions of Plk1 in early and late stages of mitosis. *Mol Biol Cell* **18**, 4024–4036.

[32] Reindl W, Yuan J, Krämer A, Krämer A, Strebhardt K, and Berg T (2008). Inhibition of Polo-like kinase 1 by blocking Polo-box domain-dependent protein-protein interactions. *Chem Biol* **15**, 459–466.

[33] Rudolph D, Steegmaier M, Hoffmann M, Grauert M, Baum A, Quant J, Haslinger C, Garin-Chesa P, and Adolf GR (2009). BI 6727, a Polo-like kinase inhibitor with improved pharmacokinetic profile and broad antitumor activity. *Clin Cancer Res* **15**, 3094–3102.

[34] Gilmartin AG, Bleam MR, Richter MC, Erskine SG, Kruger RG, Madden L, Hassler DF, Smith GK, Gontarek RR, Courtney MP, et al. (2009). Distinct concentration-dependent effects of the Polo-like kinase 1–specific inhibitor GSK461364A, including differential effect on apoptosis. *Cancer Res* **69**, 6969–6977.

[35] Lu LY, Wood JL, Minter-Dykhouse K, Ye L, Saunders TL, Yu X, and Chen J (2008). Polo-like kinase 1 is essential for early embryonic development and tumor suppression. *Mol Cell Biol* **28**, 6870–6876.

[36] Luo J, Emanuele MJ, Li D, Creighton CJ, Schlabach MR, Westbrook TF, Wong KK, and Elledge SJ (2009). A genome-wide RNAi screen identifies multiple synthetic lethal interactions with the Ras oncogene. *Cell* **137**, 835–848.

[37] Schöffski P, Blay JY, De Greve J, Brain E, Machiels JP, Soria JC, Sleijfer S, Wolter P, Ray-Coquard I, Fontaine C, et al. (2010). Multicentric parallel phase II trial of the Polo-like kinase 1 inhibitor BI 2536 in patients with advanced head and neck cancer, breast cancer, ovarian cancer, soft tissue sarcoma and melanoma. The first protocol of the European Organization for Research and Treatment of Cancer (EORTC) Network Of Core Institutes (NOCI). *Eur J Cancer* **46**, 2206–2215.

[38] Jain RJ and Stylianopoulos T (2010). Delivering nanomedicine to solid tumours. *Nat Rev Clin Oncol* **7**, 653–664.

[39] Buendia MA (2000). Genetics of hepatocellular carcinoma. *Semin Cancer Biol* **10**, 185–200.

[40] Lee JS and Thorgeirsson SS (2004). Genome-scale profiling of gene expression in hepatocellular carcinoma: classification, survival prediction, and identification of therapeutic targets. *Gastroenterology* **127**, S51–S55.

[41] Ruoslahti E, Bhatia SN, and Sailor MJ (2010). Targeting of drugs and nanoparticles to tumours. *J Cell Biol* **188**, 759–768.

[42] McMillin DW, Delmore J, Negri J, Ooi M, Klippel S, Miduturu CV, Gray NS, Richardson PG, Anderson KC, Kung AL, et al. (2011). Microenvironmental influence on pre-clinical activity of Polo-like kinase inhibition in multiple myeloma: implications for clinical translation. *PLoS One* **6**, e20226.

[43] Van de Veire S, Stalmans I, Heindryckx F, Oura H, Tijeras-Raballand A, Schmidt T, Loges S, Albrecht I, Jonckx B, Vinckier S, et al. (2010). Further pharmacological and genetic evidence for the efficacy of PlGF inhibition in cancer and eye disease. *Cell* **141**, 178–190.

[44] Studach LL, Rakotomalala L, Wang WH, Hullinger RL, Cairo S, Buendia MA, and Andrisani OM (2009). Polo-like kinase 1 inhibition suppresses hepatitis B virus X protein–induced transformation in an *in vitro* model of liver cancer progression. *Hepatology* **50**, 414–423.

[45] Petrelli A, Perra A, Schernhuber K, Cargnelutti M, Salvi A, Migliore C, Ghiso E, Benetti A, Barlati S, Ledda-Columbano GM, et al. (2012). Sequential analysis of multistage hepatocarcinogenesis reveals that miR-100 and PLK1 dysregulation is an early event maintained along tumor progression. *Oncogene*, doi: 10.1038/onc.2011.631.

Supplementary Materials and Methods

Human Tissue Samples

HCC specimen and corresponding nontumorous liver tissues were collected from 27 patients who underwent anatomic liver resection (segmentectomy or subsegmentectomy). All patients provided informed consent for tissue procurement, which was approved by the local ethics committee. Tumor characteristics were confirmed histologically to exclude mixed type of HCC. The tissue samples were snap frozen and stored at –80°C until further analyses. The patients consisted of 15 males and 12 females with a mean age of 63.8 years (standard deviation [SD], 12.0). Twelve patients had liver cirrhosis, three patients had liver fibrosis, two patients were infected with hepatitis B virus, two patients were infected with hepatitis C virus, one patient had with both viruses, and 20 patients were not infected. Adjacent healthy tissue from the same resected liver specimen served as normal tissue.

Protein Electrophoresis and Immunoblot Analysis

Homogenized tissue samples or cultured cells were lysed in RIPA buffer (25 mM Tris-HCl pH 7.6, 150 mM NaCl, 1% NP-40, 1% Na-deoxycholate, and 0.1% SDS supplemented with 10 μg/ml leupeptin and 10 μg/ml aprotinin). Equal amounts of protein were separated on SDS polyacrylamide gels as described previously [1]. Gel-resolved proteins were electrotransferred to nitrocellulose membranes and detected with anti-Plk1 (Zymed, San Francisco, CA), anti-cleaved PARP (Becton Dickinson, Sparks, MD), or anti–β-actin (Sigma-Aldrich, St. Louis, MO). Antigen-antibody complexes were visualized using appropriate horseradish peroxidase–conjugated antibodies (Santa Cruz Biotechnology, Santa Cruz, CA). In cell extracts, apoptosis was detected by anti–cleaved PARP fragment immunoblot analysis [2].

Plk1 mRNA Quantification

Total RNA was extracted from tumor, normal tissue samples, or cultured cells using the RNA Tissue Mini Kit (Qiagen, Hilden, Germany). Quantitative (TaqMan) RT-PCR for Plk1 was performed by Assays on Demand on an ABI 7000 System (Applied Biosystems, Foster City, CA). Data were normalized to the mRNA of glyceraldehyde-3-phosphate dehydrogenase coamplified with the Plk1-mRNA.

Production of Recombinant AdVs

AdVs expressing Plk1- or control-shRNAs were generated using the BLOCK-IT adenoviral RNAi expression system from Invitrogen, with the exception that, instead of the intermediate pENTR/U6 vector, we subcloned the shRNA encoding DNA sequences (Plk1: gtgcttcgagatctcggacgcggccgcgtccgagatctcgaagcactt, control hairpin: aactgggtaagcgggcgcattgatcgatcaatgcgcccgcttacccagtttt) into pALsh/H1 [3] and pDONR, followed by recombination into the pAd/BLOCK-iT-DEST vector. All subcloning steps were performed by recombination using the Gateway technology. To produce AdV-LacZ, we used the pAd/CMV/V5-GW/lacZ plasmid containing β-galactosidase under the control of a cytomegalia virus (CMV) promoter (Invitrogen). The pAd/BLOCK-iT-DEST and pAd/CMV/V5-GW/lacZ constructs (approximately 34 kb) were linearized with *Pac* I (New England Biolabs, Ipswich, MA) and transfected into HEK 293A cells using Lipofectamine 2000 (Invitrogen). Adenoviral particles were harvested by subjecting the HEK 293A cells to three freeze/thaw cycles. The recombinant adenoviral particles were purified by a two-step CsCl

purification, filtration through a PD-10 desalting columns loaded with Sephadex G-25 (Amersham, Uppsala, Sweden), and titered by a plaque assay. For adenoviral infection, cells were grown to 50% to 70% confluence in 24-well plates. AdV type 5 was mixed with 300 μl of complete medium to a concentration of 0.1 to 1×10^5 pfu/ml and added to the cells. After 6 hours, the medium was replaced by complete medium.

Cell Viability Assay

To determine the number of viable cells, we used the 3-(4,5-dimethylthiazol-2-yl)-2,5-diphenyltetrazolium bromide (MTT, Sigma-Aldrich) colorimetric assay [4].

Detection of Apoptosis

In cell culture experiments, apoptosis was evaluated using a Zeiss 35315 fluorescent microscope by inspection of nuclear morphology and appearance of clear condensed chromatin characteristic of apoptotic cells after staining with the blue fluorescent dye Hoechst 33342 (Sigma-Aldrich). This dye stains the condensed chromatin of apoptotic cells more brightly than the chromatin of normal cells. Quantification of apoptotic cells was performed on images taken from at least four representative areas for each condition. For each condition, at least 1400 cells were evaluated.

FACS Analysis

Cell cycle distribution was analyzed using a Becton Dickinson FACScan apparatus (Becton-Dickinson, La Jolla, CA) and the Cell-Quest 3.1 software as described [5]. The cells were harvested, washed with PBS, fixed with ethanol, and stained with propidium iodide. For each experiment, the cells were analyzed in triplicate. The integrity of the cell population, the duplet discrimination, and the statistical analyses were performed using the WinMDI software (http://facs.scripps.edu/software.html).

Immunocytochemistry

To visualize cell division spindles, cells were grown on coverslips and fixed with methanol at –20°C for 10 minutes. After fixation, samples were washed with PBS and permeabilized with 0.01% Triton X-100 in PBS for 30 seconds, washed again, and thereafter blocked with 1% BSA in PBS for at least 1 hour. Coverslips were incubated for 1 hour at room temperature with anti–α-tubulin (clone B-5-1-2; Sigma-Aldrich) 1:500 and consecutively with a secondary antibody (Alexa Fluor 594 donkey antimouse; Invitrogen) and DAPI (Invitrogen). After washing, the coverslips were mounted with anti-fading mounting solution (Invitrogen) onto the slides. Images were taken on a Zeiss Axioplan 2 microscope equipped with a CCD camera (Zeiss, Oberkochen, Germany).

Immunohistochemistry

For histopathologic studies, dissected organs were fixed in 10% buffered formalin and embedded in paraffin. Paraffin sections (3 μm) were stained with hematoxylin-eosin, and hepatocellular lesions were graded as foci of altered hepatocytes or adenomas.

For immunostaining, tissue sections were incubated with specific antibodies against Ki-67 (ready-to-use; Master Diagnostica, Granada, Spain). Antigen retrieval was performed with PT Link (Dako, Glostrup, Denmark) in 10 mM citrate buffer, pH 6.1. The samples were then incubated for 1 hour at room temperature with the primary antibody. Immunostainings were performed using goat antirabbit horseradish

peroxidase (Dako) as secondary antibody. Tissue sections were subsequently incubated with a polymer-peroxidase complex and 3,3′-diaminobenzidine, and counterstained with hematoxylin (ChemMate, Dako). Some sections were incubated without the primary antibody as negative controls. Mouse intestine and embryo specimens that had previously shown a marked positivity for each antibody were also routinely included as positive controls. Digital slides and representative pictures of liver nodules were obtained with a Mirax scan (Zeiss).

Determination of the Levels of BI 2536 in Mouse Tissue

Eight TGFα/*c-myc* mice received 30 mg/kg BI 2536 intravenously. At each of the four different time points (0.5, 2, 6, or 12 hours after injection), two mice were terminally anesthetized and perfused with Ringer's solution to remove the remaining BI 2536 from the blood vessels. Samples of liver and HCC tissue from each mouse were snap frozen in liquid nitrogen and stored at −80°C. The concentrations of BI 2536 in tumor and liver tissue were analyzed by mass spectrometry by Pharmacelsus (Saarbrücken, Germany).

Determination of Blood Perfusion of Liver and HCC Tissue in TGFα/c-myc Mice

Contrast-enhanced MRI using the intravascular contrast agent, Glowing *Ga*lbumin-Rhodamine B (Biopal, Worcester, MA), was done in a 3-T MRI scanner [6]. Six tumor-bearing mice were anesthetized, and MRI images were obtained before and after intravenous injection of 100 µl of Glowing *Ga*lbumin-Rhodamine B. The animals were imaged in the coronal plane using a T1-weighted, 3D FLASH sequence as described recently [6]. Contrast enhancement of tumor normalized to liver was calculated using the following formula: contrast enhancement$_{tumor}$ / contrast enhancement$_{liver}$ = signal intensity$_{tumor}$ (Galbumine) − signal intensity$_{tumor}$ (nativ)/signal intensity$_{liver}$ (Galbumine) − signal intensity$_{liver}$ (native). Subsequently, the mice were sacrificed, and the livers were excised and fixed for 24 hours in 4% paraformaldehyde solution. Cryosections from each liver containing HCC and normal liver tissue were analyzed by confocal laser scanning microscopy with an Olympus FluoView FV-1000 (Olympus Europe, Hamburg, Germany). Rhodamin B fluorescence was excited at 543 nm, and emitted light was detected from 550 nm to 650 nm. The autofluorescence of liver tissue (excitation at 488 nm, emission at 500-530 nm) was used to visualize liver tissue.

Data Presentation and Statistical Analysis

Unless otherwise stated, all cell culture experiments were performed at least on three different occasions with similar results. The values are given as means ± SD. Data from different treatment groups were analyzed by the Student's *t* test for unpaired samples using the SPSS 16.0 software or Fisher exact test. Values of cell viability, tumor volume, and tumor mass were assumed to be normally distributed. Ratios and values of the percentage of apoptotic cells and of mRNA quantification were assumed to be log normally distributed. $P < .05$ was considered to indicate statistical significance (*).

Supplementary References

[1] Laatsch A, Ragozin S, Grewal T, Beisiegel U, and Joerg H (2004). Differential RNA interference: replacement of endogenous with recombinant low density lipoprotein receptor–related protein (LRP). *Eur J Cell Biol* **83**, 113–120.

[2] Haupenthal J, Baehr C, Zeuzem S, and Piiper A (2007). RNAse A–like enzymes in serum inhibit the anti-neoplastic activity of siRNA targeting Polo-like kinase 1. *Int J Cancer* **121**, 206–210.

[3] Lazebnik YA, Kaufmann SH, Desnoyers S, Poirier GG, and Earnshaw WC (1994). Cleavage of poly(ADP-ribose) polymerase by a proteinase with properties like ICE. *Nature* **371**, 346–347.

[4] Mosmann T (1983). Rapid colorimetric assay for cellular growth and survival: application to proliferation and cytotoxicity assays. *J Immunol Meth* **65**, 55–63.

[5] Kiermayer S, Biondi RM, Imig J, Plotz G, Haupenthal J, Zeuzem S, and Piiper A (2005). Epac activation converts cAMP from a proliferative into a differentiation signal in PC12 cells. *Mol Biol Cell* **16**, 5639–5648.

[6] Korkusuz H, Knau LL, Kromen W, Bihrer V, Keese D, Piiper A, and Vogl TJ (2012). Different signal intensity at Gd-EOB-DTPA compared with Gd-DTPA–enhanced MRI in hepatocellular carcinoma transgenic mouse model in delayed phase hepatobiliary imaging. *J Magn Reson Imaging*, doi: 10.1002/jmri.23584.
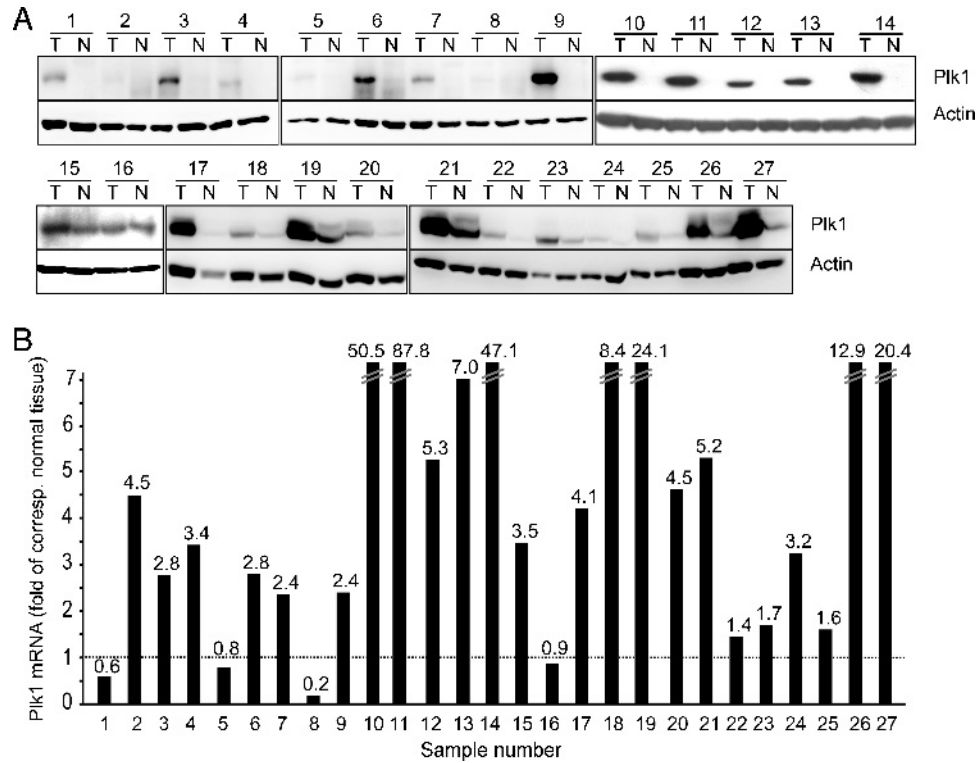
Figure W1. Plk1 is frequently overexpressed in human HCCs. 27 pairs of HCCs (T1-T27) and corresponding noncancerous liver tissues (N1-N27) were obtained by surgery. (A) Protein was extracted from the tissue samples and was analyzed by anti-Plk1 and anti–β-actin immunoblot analysis. (B) Determination of Plk1 mRNA by quantitative PCR. Expression levels of Plk1 mRNA were normalized against glyceraldehyde-3-phosphate dehydrogenase. Data represent Plk1 mRNA levels in HCC tissue samples divided by the Plk1 mRNA level in normal liver tissue of the same patient. The numbers above the columns indicate the fold Plk1 in the HCC sample of the corresponding noncancerous tissue.
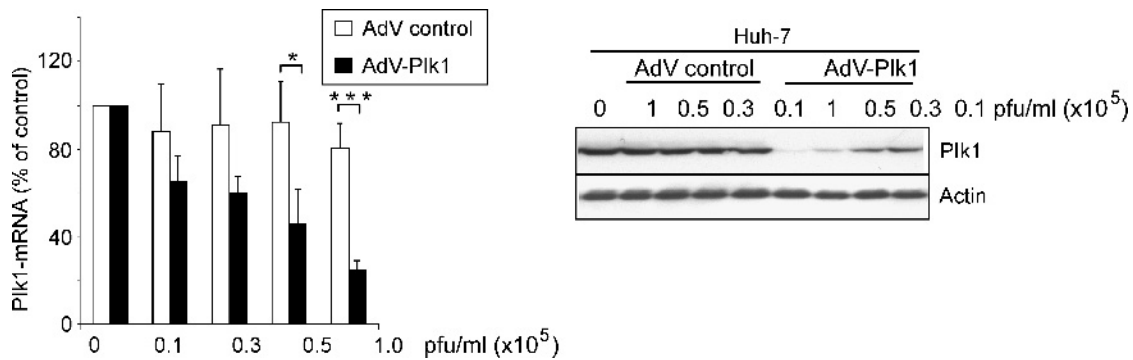

Figure W2. AdV-Plk1, but not AdV control, inhibited Plk1 expression in cultured HCC cell lines. Huh-7 cells were infected with 10^5 pfu/ml or the indicated amount of AdV-Plk1 or AdV control. At 48 hours later, the cells were lysed and analyzed for Plk1 mRNA (left panel) as well as by anti-Plk1 and anti–β-actin immunoblot analysis (right panel). Asterisks (*) indicate a significant difference between control AdV– and AdV-Plk1–treated cells.
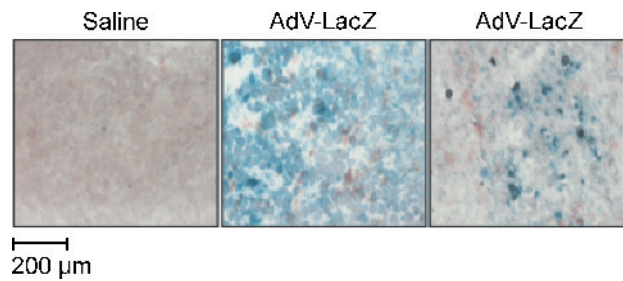
Figure W3. Intravenously infused AdV effectively infects Huh-7 tumors in nude mice. When the tumors reached a diameter of 2 to 3 mm, 300 μl (7×10^9 pfu) of AdV-LacZ suspension or saline were injected intravenously. Three days later, the mice were sacrificed, and the tumors were excised. Cryosections were stained with X-Gal and counterstained with Nuclear Fast Red. Pictures were taken using a CCD camera and reveal that xenografts from AdV-LacZ–treated animals but not from saline-treated animals showed significant X-Gal staining. Magnification, $\times$200.
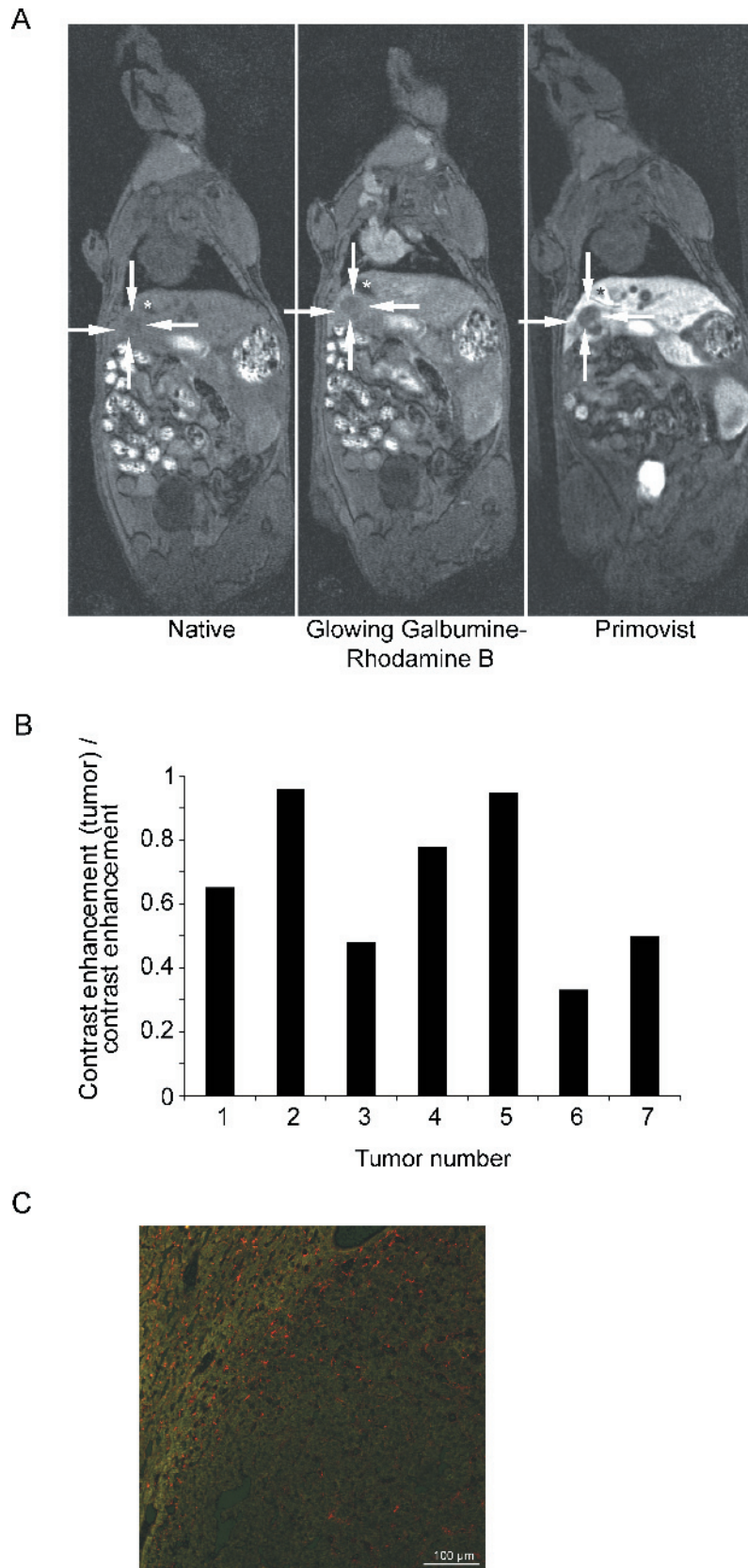
Figure W4. Tumors of TGFα/*c-myc* mice are frequently less perfused than normal liver tissue. (A) MR images of a tumor-bearing HCC before (native) and after intravenous injection of 100 μl of Glowing Galbumine-Rhodamine B (middle panel). The right panel shows the same tumor by Primovist-enhanced MRI 1 week before. The tumor is marked by arrows. Gallbladders are marked by asterisks. (B) Ratios of contrast enhancement of tumor and corresponding normal liver tissue in the six TGFα/*c-myc* mice. Numbers 2 and 3 are two different tumors of the same mouse. (C) Confocal laser scanning microscopy image of a cryosection from the same mice as (A) and (B). The tumor tissue (lower right part) shows less and a more heterogeneous staining with Rhodamine B (red) compared with the normal liver tissue (upper left part).